Stability and operation limits of power systems with high penetration of power electronics

Carlos Collados-Rodriguez [*], Marc Cheah-Mane, Eduardo Prieto-Araujo, Oriol Gomis-Bellmunt

CITCEA-UPC, ETSEIB Av. Diagonal 647, 08028, Barcelona, Spain

ARTICLE INFO

ABSTRACT

Modern power systems are facing a number of challenges related to stability when integrating large amounts of power electronics, which is present in renewable generation, energy storage, flexible AC transmission systems or high voltage DC links. This paper analyses the stability and operation limits in power systems with high penetration of power electronics. In particular, steady-state, small-signal and transient analysis have been carried out to examine the minimum synchronous generation required to ensure stability in presence of an HVDC link based on a VSC operating in grid-following control. These analysis are based on performance indices, which evaluate the main magnitudes of the system, such as the grid frequency and voltage, but also the particular magnitudes of the system elements, mainly generators and VSCs. The use of these indices provides a fast overview of the system performance that could lead to save analysis time of power system engineers in the task of identifying critical cases for the system.

1. Introduction

The installation of new renewable generation, HVDC interconnections, storage, FACTS and active loads, such as electrical vehicle, is increasing the number of power-electronics units connected to power systems. The high penetration of converters is transforming the power systems, posing important challenges for Transmission System Operators (TSOs). Recently, several instability incidents have been reported around the world. In [1–3] a number of interaction events in China due to subsynchronous resonances have been studied in detail. Harmonic frequency interactions between the export cables and the HVDC-connected wind power plant BorWin1 were presented in [4]. In addition, severe fault events have been reported in systems with a high number of power electronics units. Power outages occurred after cascaded trips in South Australia in 2016 [5] and 2018 [6] and in the UK in 2019 [7]. It is clear that power electronics is introducing new dynamics into power systems, leading to new instability mechanisms. Then, power converter based power systems need to be studied in detail, specially considering transient contingencies, to understand their operation and to adequate the protection systems.

A number of publications have addressed stability analysis considering a conventional generation displacement due to an increase of converter based generation. The Irish island has been widely studied in [8–10]. The power system stability was evaluated in [8] modifying the penetration of wind power generation. In particular, a power flow and small-signal analysis were carried out, but the main findings are related to the frequency excursions after transient events, *e.g.* loss of the largest infeed and faults. In [9], the steady-state voltage stability was investigated using a probabilistic power flow to determine the maximum instantaneous wind power penetration, while transient stability was considered in [10]. Voltage stability is analysed in [11], providing also a maximum active power capability for converters connected to weak grids. Moreover, the impact of storage systems with high penetration of solar and wind generation was analysed in the French island of Guadeloupe using dynamic simulations [12]. The effect of converter based generation increase on electromechanical oscillation modes has been evaluated in [13,14]. Specifically, the eigenvalue sensitivity to the system inertia is investigated when the DFIG-based wind power is increased in [13], while [14] considers the effect of distributed PV systems. The impact of Power Oscillation Damping (POD) of wind turbines in low-inertia systems is evaluated in [15]. In particular, most of publications focused on the frequency stability due to the inertia reduction, while the reduction of synchronous generation can also involve other issues due to lower short-circuit current capability or voltage regulation.

This paper extends the authors' previous work [16], where the stability of an essential system was investigated when the synchronous generation was progressively reduced considering grid-following operation for the converter. That study was focused on a small-signal analysis, specifically evaluating the oscillation modes and participation
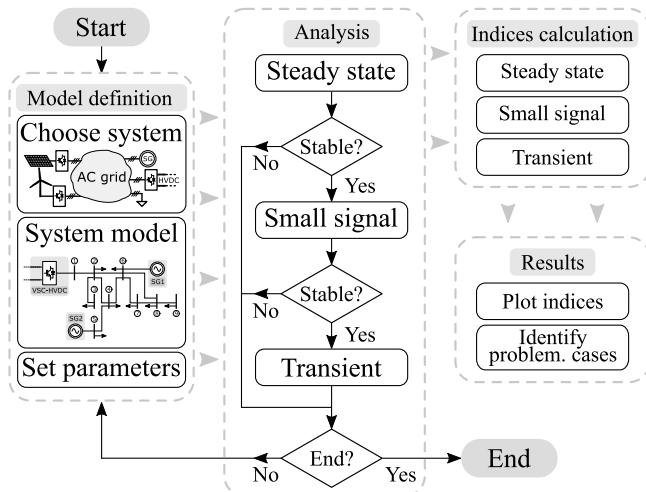
Fig. 1. Flowchart of the index-based methodology.

factors of the system. In particular, this publication provides more insights for the following aspects:

- Transient stability analysis and operation limits are evaluated for a power system with a Voltage Source Converter (VSC) operating in grid-following mode when the Synchronous Generator (SG) presence is reduced, identifying if new control algorithms, *e.g.* grid-forming, are needed to overcome these limitations.
- This analysis has been applied to a larger system. In particular, the minimum SG size that ensures a proper system operation is identified for a 9-bus system in presence of two SGs and a VSC-HVDC link.
- The operation limits have been defined based on steady-state, small-signal and transient analysis using performance indices, which can help to simplify the analysis of several cases, reducing the analysis time for power system engineers.
- A global stability map has been generated based on previous performance indices. In this paper, this map has been built based on two variables, the rated power of two SGs, leading to a two-dimensional map, which highlights the steady-state, small-signal and transient unstable operation areas for the previous 9-bus system.

2. Methodology to study system stability and operation limits

In this section, a methodology to analyse power system stability and assess the operation limits is introduced. This methodology is based on performance indices, which allow to evaluate the main magnitudes of the system, such as the frequency or the voltage, but also the properties of the particular system elements, such as the rotor angle of a Synchronous Generator (SG) or the PLL synchronism of a VSC.

The starting point of the methodology is the model definition, where the system models and parameters are introduced. A power flow model, a linear dynamic model and a non-linear dynamic model of a specific system have to be provided to carry out the analysis. The system analysis is structured in three levels that provide different information: steady-state analysis, small-signal analysis and transient analysis, as shown in the flowchart in Fig. 1.

This methodology starts analysing the static operation point of the system, looking at the generator angles, bus voltages and load level considering current capacity of each element. If the system achieves a feasible equilibrium point, then the small-signal analysis is performed. Then, if the system is stable, *i.e.* all poles have positive damping, time-domain simulations are performed to evaluate the system response

after transient events, such as faults, generators trips or grid topology variations. Each analysis level outputs several indices that provide information about the stability and operation limits of the system. All the indices have been normalised between 0 and 1, such that values close to 0 refer to normal operation or low risk of instability, while values above 1 indicate instabilities or operation limit violations. The indices combination is used to identify potential problematic cases that later can be studied in detail. This methodology allows reducing the number of transient time-domain simulations because steady state and small-signal analysis are used to discard part of the unstable cases. The indices can be used to analyse many cases evaluating a reduced number of electrical or stability magnitudes, which leads to a reduction of analysis time for power system engineers.

2.1. Model definition

In this paper, a power system with high penetration of power electronics is considered. This system might include synchronous generators, representing classic thermal power plants, and VSCs, modelling wind or solar power plants or HVDC links. The SG is modelled using the electrical machine and turbine dynamic equations along with the exciter and governor controls. The exciter model implemented in this paper is the AC4 [17], while the governor includes a conventional frequency droop control. The VSC is represented using an average model and a conventional grid-following control structure is assumed. As shown in Fig. 2, the grid-following control includes a Phase Locked Loop (PLL), an inner current loop, an AC voltage control, an active power control and a frequency droop control. Other control approaches could be also considered for the VSC [18], such as PQ operation mode, AC voltage droop or include inertia emulation in the frequency control [19].

The lines are represented as π equivalents while the loads are modelled as constant impedances. A more detailed description about the modelling of the system elements can be found in [16]. For the steady-state analysis, some assumptions are considered, leading to the following power flow models of the SG and VSC:

- Synchronous generator: the *classical model* defined in [20] is used. The SG is represented as an internal bus voltage E with an impedance X_{sg}, which corresponds to the sum of the leakage stator impedance and the mutual inductance. The internal voltage E depends on the field current i_{fd}, such that $E = X_{sg} i_{fd} = X_{sg} v_{fd}/R_{fd}$, where v_{fd} is the field winding voltage applied by the exciter and R_{fd} is the field winding resistance. This model provides fast computational solutions, while ensuring high accuracy. In case of SG defined as slack bus, $\delta_{sg} = 0°$ is added as angle restriction.
- VSC: representation as PQ or PV buses can be considered depending on the converter control mode. The frequency droop control can be also implemented.

2.2. System analysis

The system analysis is structured in three levels: steady-state analysis, small-signal analysis and transient analysis.

2.2.1. Steady-state analysis

This first approach allows to identify steady-state operation limits through power flow analysis [20]. Three indices related to the static results are defined:

- Generator Angle Index (GAI) [21]: shows the highest rotor angle among the n_g generators of the system in relation to a maximum admissible value δ_{adm}. The maximum admissible angle δ_{adm} selected in this paper is 90°, which corresponds to the steady-state stability limit. However, other values could be used. In [21], the
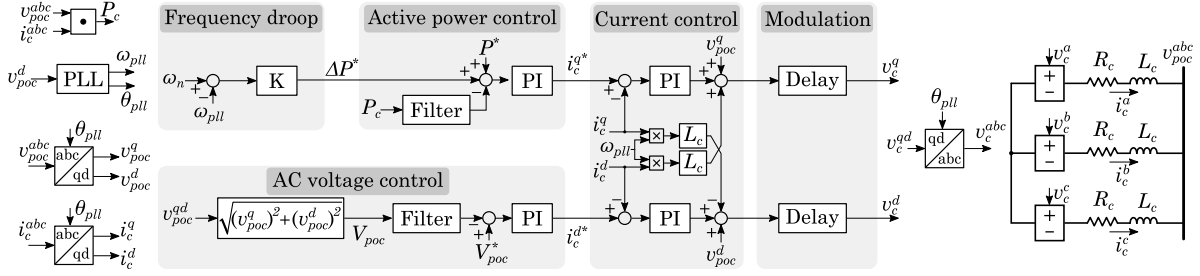
Fig. 2. VSC average model and implemented grid-following control.

maximum admissible angle was set to 120°, which is a typical value used to adjust the load angle protections of synchronous generators.

$$\text{GAI} = \frac{\max\left(\delta_1, \ldots, \delta_{n_g}\right)}{\delta_{adm}}, \quad \delta_{adm} = 90° \tag{1}$$

- Voltage Index (VI): shows the maximum voltage deviation among the n_b buses of the system in relation to a maximum admissible value Δv_{adm}:

$$\text{VI} = \frac{\max\left(|1 - v_1|, \ldots, |1 - v_{n_b}|\right)}{\Delta v_{adm}}, \quad \Delta v_{adm} = 0.1 \text{ pu} \tag{2}$$

- Current Index (CI): is the maximum current in relation to the nominal value among the n_k elements of the same k category:

$$\text{CI}_k = \max(I_{k-1}/I_{k-1}^{nom}, \ldots, I_{k-n_k}/I_{k-n_k}^{nom}) \tag{3}$$

where k, in this paper, corresponds to three categories: generators g, converters c and lines l. In case of the generators, only the armature current limit has been considered.

2.2.2. Small-signal analysis

The small-signal analysis includes the linear dynamic response of the power system components, e.g. converter control algorithms. The main mechanisms of instability and interactions can be identified from the eigenvalues and Participation Factors (PFs), which are obtained from a state-space model of the system. The initial conditions of the state-space model are defined by the operation points obtained from the previous power flow analysis. In particular, the power flow provides the magnitude and angle of the bus voltages and the active and reactive power exchange between buses. The linear system requires as inputs the initial values of voltages and currents expressed in the qd reference frame. In this manuscript, the rotor of the SG connected to the slack bus is used as reference for the qd frame, referred as Grid Reference Frame (G-RF). Then, the bus voltages can be expressed in the G-RF as:

$$v_{i0}^q = \sqrt{\frac{2}{3}} V_b v_i \cos\left(\delta_i\right), \quad v_{i0}^d = -\sqrt{\frac{2}{3}} V_b v_i \sin\left(\delta_i\right) \tag{4}$$

where v_i and δ_i are the magnitude and angle of the i-bus voltage from the power flow solution and V_b is the base RMS voltage used to calculate the pu magnitudes. Line currents can also be expressed in the G-RF. First, the RMS value of the current through each of the n_l lines can be calculated as:

$$I_l = \frac{\sqrt{P_{l-i}^2 + Q_{l-i}^2}}{\sqrt{3} V_b v_i}, \quad \forall l \in [1, n_l] \tag{5}$$

where P_{l-i} and Q_{l-i} are the active and reactive power flowing through the line l from the bus i. Then, the qd components of the currents can be obtained as:

$$i_{l0}^q = \sqrt{2} I_l \cos\left(\delta_i - \phi_{l-i}\right), \quad i_{l0}^d = -\sqrt{2} I_l \sin\left(\delta_i - \phi_{l-i}\right) \tag{6}$$

where ϕ_{l-i} is the angle between the i-bus voltage and the l-line current, which is calculated as:

$$\phi_{l-i} = \cos^{-1}\left(\frac{P_{l-i}}{\sqrt{P_{l-i}^2 + Q_{l-i}^2}}\right) \text{sign}\left(\frac{Q_{l-i}}{P_{l-i}}\right) \tag{7}$$

Three more indices have been defined based on the damping ratio and PF matrix provided by the small-signal analysis:

- Damping Index (DI): indicates the minimum damping ξ of the M system modes:

$$\text{DI} = 1 - \min(\xi_1, \ldots, \xi_M) \tag{8}$$

An index value higher than 1 indicates an instability.
- Interaction Index (InI): reveals interactions between two elements from different categories, i.e. SGs, VSCs and lines. The InI of each mode m is calculated as the geometric average of the maximum PF within the elements of each category:

$$\text{InI}_m = \sqrt{\max(PF_{m-k_1})^2 + \max(PF_{m-k_2})^2}, \quad \forall m \in [1, M] \tag{9}$$

where k_1 and k_2 with $\forall k_1, k_2 \in \{g, c, l\}$ and PF_m is the vector of PFs of each mode m. Then, a value equal to zero corresponds to no interaction while an index close to 1 indicates a strong interaction between two elements. Also, the maximum interaction of the system is defined as $\text{InI} = \max(\text{InI}_1, \ldots, \text{InI}_M)$.
- Risky Interaction Index (RInI): extends the InI considering also the damping ratio, revealing interactions that can be potentially unstable. Then, the RInI for each mode m is expressed as:

$$\text{RInI}_m = \left(1 - \xi_m\right)\sqrt{\max(PF_{m-k1})^2 + \max(PF_{m-k_2})^2}, \quad \forall m \in [1, M] \tag{10}$$

2.2.3. Transient analysis

Time-domain simulations are the most accurate method to assess the stability of a power system. It allows the study of transient events, such as SG disconnections or faults, which cannot be analysed with the previous methods. However, this approach requires greater computational effort and time. Six indices are defined from time-domain simulations results:

- Dynamic Generator Angle Index (DGAI): indicates the maximum rotor angle reached by the n_g SGs after a transient event, determining how close the SG is from losing synchronism. This index has the same definition (1) as the GAI. During a fault, the SG angle can reach high values, preventing the recognition of the synchronisation loss. Then, this index is calculated considering the maximum SG angle 100 ms after the fault clearance.
- Dynamic Voltage Index (DVI): it is based on [21], but here it is defined to analyse the overvoltage after a transient event. Then, only bus voltage deviations above 1 pu are considered and DVI is calculated in relation to an admissible voltage deviation Δv_{adm}:

$$\text{DVI} = \frac{\max(1, \max(v_1, \ldots, v_{n_b})) - 1}{\Delta v_{adm}}, \quad \Delta v_{adm} = 0.1 \text{ pu} \tag{11}$$

(a) Generic scheme

(b) State-space model
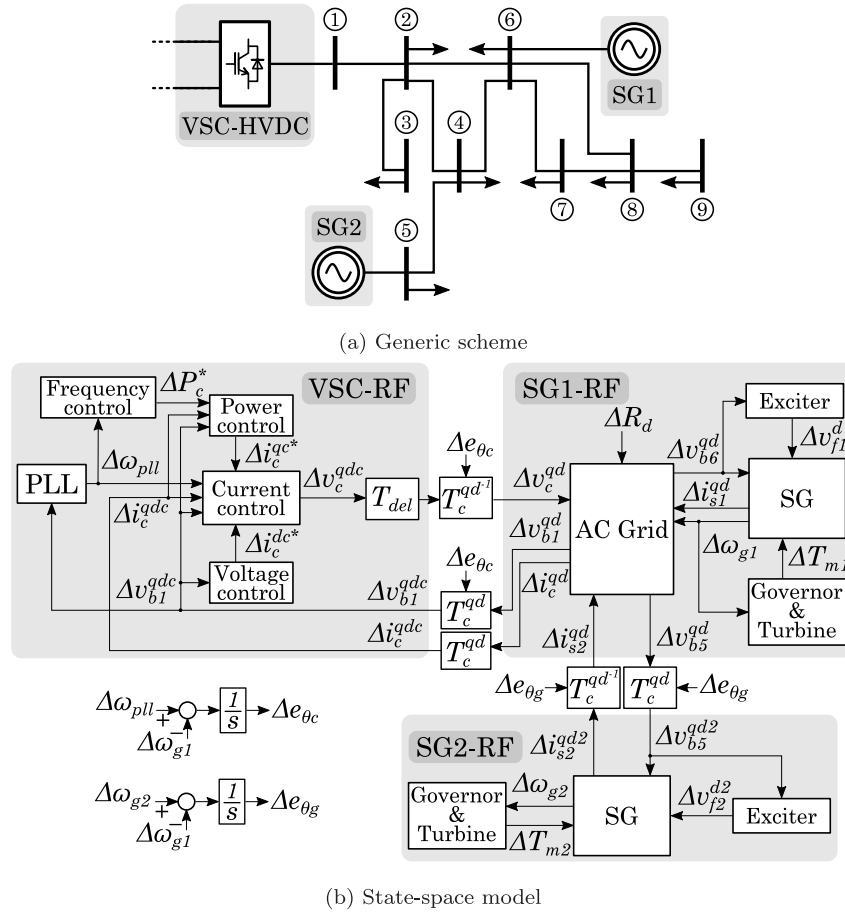
Fig. 3. Island 9-bus system.
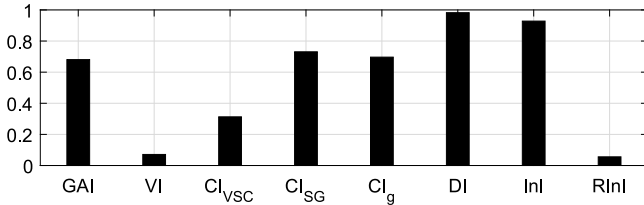
Fig. 4. Steady-state and small-signal indices obtained for Case 1.

- Dynamic Current Index (DCI): is equivalent to the definition of CI in (3), but applied to time domain results.
- Maximum Frequency Deviation Index (MFDI): shows the maximum SG frequency deviation from the nominal value after a transient event in relation to a maximum admissible value Δf_{adm}:

$$\text{MFDI} = \frac{\max(|\Delta f_1|, \ldots, |\Delta f_{n_g}|)}{\Delta f_{adm}}, \quad \Delta f_{adm} = 1 \text{ Hz} \quad (12)$$

- Frequency Derivative Index (FDI): shows the maximum frequency derivative reached by the SGs, which is measured within a time window of 0.5 s [22,23]. The maximum admissible value depends on the specific system under study, i.e. this is set by the TSO. Currently, the ROCOF protections in isolated systems are set at 1 Hz/s, such as Ireland [22] and UK [23]. However, higher ROCOF levels, as 1.5 or 2 Hz/s, are also considered as safe limits for SGs [24,25]. As an example, a maximum admissible ROCOF

equal to 2 Hz/s is adopted. Then, the FDI is expressed as:

$$\text{FDI} = \frac{\max(|\Delta f_1|/\Delta t, \ldots, |\Delta f_{n_g}|/\Delta t)}{\Delta f_{adm}/\Delta t}, \quad \Delta f_{adm}/\Delta t = 2 \text{ Hz/s} \quad (13)$$

- PLL Index (PLLI): reveals the maximum deviation of the frequency measured by the PLL of the converters. The definition of PLLI is the same as (12) for MFDI. This deviation could be caused by a deviation of the actual system frequency or by a VSC loss of synchronism. Analytical expressions to evaluate how close is the PLL to lose synchronism based on the fault depth are suggested in [26,27], which could save simulation time.

3. Case studies

In this section, the methodology described in the previous section have been applied to a power system based on the 220 kV grid of the Mallorca island. This island system is modelled as a 9-bus grid, shown in Fig. 3(a), including two classic thermal power plants connected to buses 5 and 6 and a VSC-HVDC link connected to bus 1. The complete state-space model of the system is also represented in Fig. 3(b).

Two case studies are analysed, considering a high presence of synchronous generation (Case 1) and a reduction of synchronous generation (Case 2). The SGs active power reference is set to 70% of their rated power, while the VSC-HVDC link provides the rest of the demand. Then, the previous methodology has been applied for these two case studies to exemplify how the indices can help to analyse the system operation. The contingencies considered for the transient analysis are the SG2 disconnection and a three-phase fault located in bus 6.
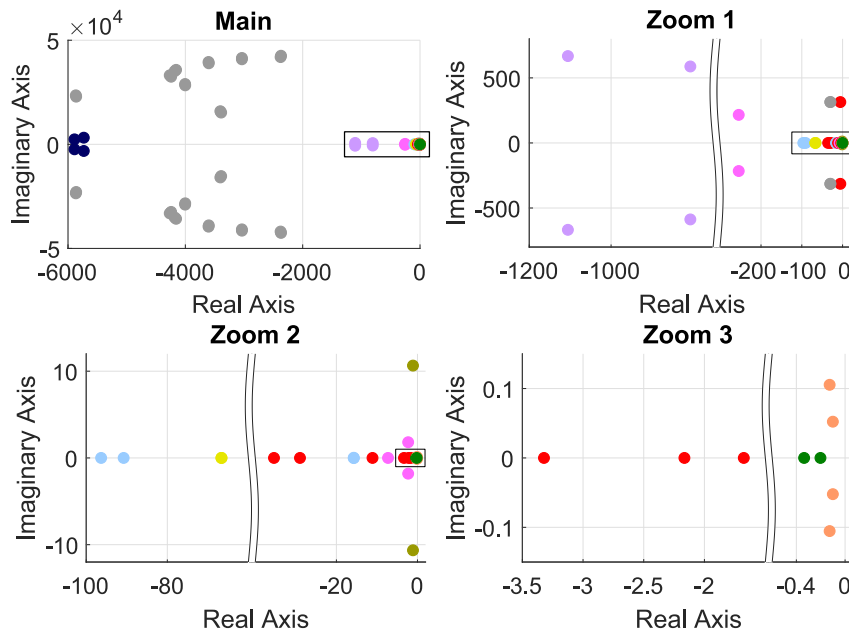
Fig. 5. Pole diagram of Case 1.

Table 1
Parameters for cases 1 and 2.

Parameter	Symbol	Case 1	Case 2	Unit
SG1 rated power	S_{SG1}	250	100	MVA
SG2 rated power	S_{SG2}	250	100	MVA
VSC rated power	S_{VSC}	500	500	MVA
Total system demand	P_{load}	500	500	MW

Table 2
Comparison of power flow and simulation results of case 1.

Mag.	P. flow	Sim.	Mag.	P. flow	Sim.
v_1 (pu)	1.0000	1.0000	δ_1 (°)	0.573	0.573
v_2 (pu)	0.9956	0.9956	δ_2 (°)	0.041	0.041
v_3 (pu)	0.9953	0.9953	δ_3 (°)	−0.220	−0.220
v_4 (pu)	0.9940	0.9940	δ_4 (°)	0.072	0.072
v_5 (pu)	0.9929	0.9929	δ_5 (°)	0.362	0.362
v_6 (pu)	0.9934	0.9934	δ_6 (°)	0	0
v_7 (pu)	0.9932	0.9932	δ_7 (°)	−0.274	−0.274
v_8 (pu)	0.9932	0.9932	δ_8 (°)	−0.324	−0.324
v_9 (pu)	0.9929	0.9929	δ_9 (°)	−0.510	−0.510
δ_{sg1} (°)	−61.27	−60.12	δ_{sg2} (°)	−54.48	−53.50
P_{sg1} (MW)	173.3	173.4	Q_{sg1} (Mvar)	−53.8	−53.8
P_{sg2} (MW)	173.4	173.4	Q_{sg2} (Mvar)	−25.0	−25.0
P_{vsc} (MW)	147.3	147.4	Q_{vsc} (Mvar)	52.3	52.3
f (Hz)	50.013	50.013			

Table 3
Pole characteristics in case 1.

Pole	Group/s	f [Hz]	ξ	InI	RInI
1–32	Grid	2427–6772	0.056–0.25	0.09	0.06
33–36	VSC	380.3–507.2	0.87–0.93	0.27	0
37–40	VSC-SG	93.5–106.3	0.81–0.86	0.93	0.03
41–44	Grid	50.01	0.10	0	0
45–46	SG	50.00	0.018	0	0
47–48	VSC-SG	34.34	0.76	0.61	0.03
49–50	VSC	0	1	0.28	0
51–52	SG Exc	0	1	0	0
53–54	Isg	0	1	0.26	0
55–56	Mechs	1.69	0.10	0.03	0.03
57–58	VSC	0	1	0.07	0
59	Isg	0	1	0.12	0
60–62	Ivsc-Isg	0–0.29	0.79–1	0.83	0.03
63–65	Isg	0	1	0.41	0
66–67	Mechs	0	1	0.20	0
68–71	Exc-Isg	0.008–0.017	0.77–0.89	0.47	0.03

3.1. Case 1: high presence of synchronous generation

This first case study considers that the SG-based installed capacity is equal to the rated power of the VSC-HVDC link, which is 500 MVA, as shown in Table 1. Then, both SGs generate 350 MW (70%) of the demand, while the VSC supplies the rest, *i.e.* 150 MW (30%).

Following the methodology, the steady-state analysis is carried out first. The power flow results are shown in Table 2, which gathers the bus voltages (magnitude and angle), the rotor angle of the SGs, the active and reactive power injected by the SGs and VSC and the system frequency. An stable operation point is reached, with a very low bus voltage and frequency deviations. The maximum voltage deviation is found in buses 5 and 9, which show a voltage equal to 0.9929 pu, resulting in a VI of 0.071 in Fig. 4. The rotor angle of the SGs is also within normal values, around 50–60° [20], which is equivalent to a GAI of 0.68. The indices related to the currents, CI_{VSC}, CI_{SG} and CI_g, show that there is no overload in any of the elements of the system, as all of them are lower than 0.8. Therefore, the indices show that the maximum admissible limits of steady state operation are not exceeded.

In addition, the power flow results have been compared to the steady state points obtained from the time-domain simulation in Table 2. Only the rotor angles of the generators differ (difference less than the 2%) due to the simplified representation of the SGs. This comparison validates both models for the small-signal and transient analysis.

Then, the small-signal analysis is applied considering the power flow results as the initial values of the state variables. The poles and the PF matrix are represented in Figs. 5 and 6, respectively, using the same colours for each group. In case of the PFs in Fig. 6, dark colours show a high participation of a variable in a specific mode. Note that the participation of a variable in the different modes of the system corresponds to each row of rectangles. The variables have been grouped

in different names for clarity, *e.g.* I_{vsc} groups the qd converter currents or I_{sg} groups all the SG currents also expressed in the qd reference frame. Also, the poles characteristics are shown in Table 3, where poles are arranged according to the frequency, including the damping and small-signal indices.
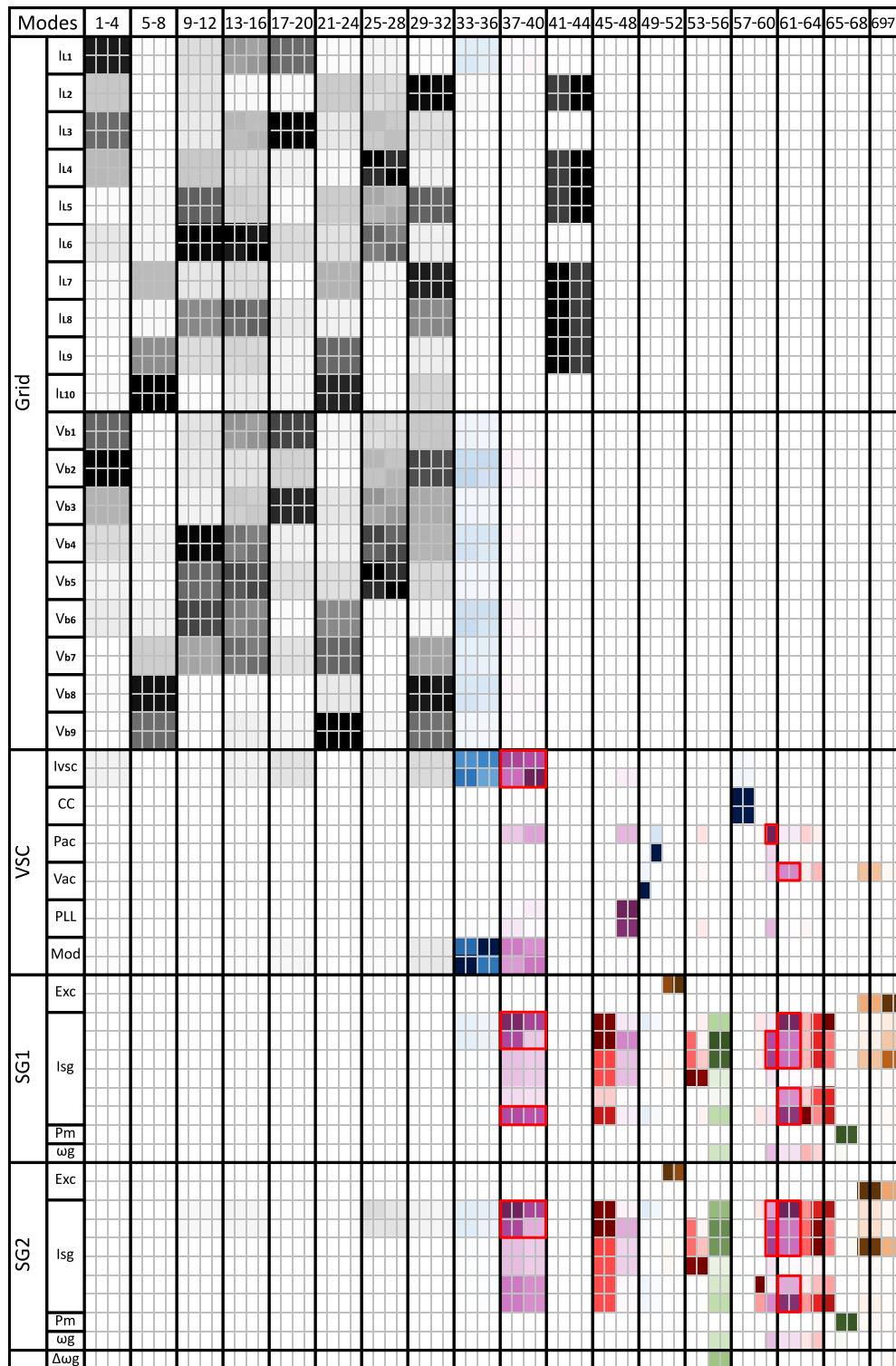
Fig. 6. Participation factor matrix of Case 1.

The PF matrix in Fig. 6 reveals strong interactions between the VSC and the SGs, as observed in poles 37–40, with participation of VSC and SG currents, and poles 60–62, with participation of VSC active power and AC voltage control and SG currents. The participating variables in each of the previous oscillation modes, *i.e.* the variables with highest PFs (darkest colour), have been highlighted with a red square in the PF matrix shown in Fig. 6. These interactions are also indicated in the InI with values equal to 0.93 for poles 37–40 and 0.83 for poles 60–62. However, the risk of instability of these modes is very low, as

they present a high damping (around 0.8 in Table 3), resulting in a very low RInI equal to 0.06. Besides, modes related to the SG currents (poles 45 and 46) show the lowest damping of the system, which is equal to 0.018, leading to a DI very close to 1 (0.982). Therefore, the indices clearly identify interactions between the SGs and the converter and confirm that the system is stable.

Finally, the transient analysis is carried out with EMT time-domain simulations. The system remains stable for the fault at bus 6 and SG2 disconnection, as observed in Figs. 7 and 8. In the fault case, the VSC
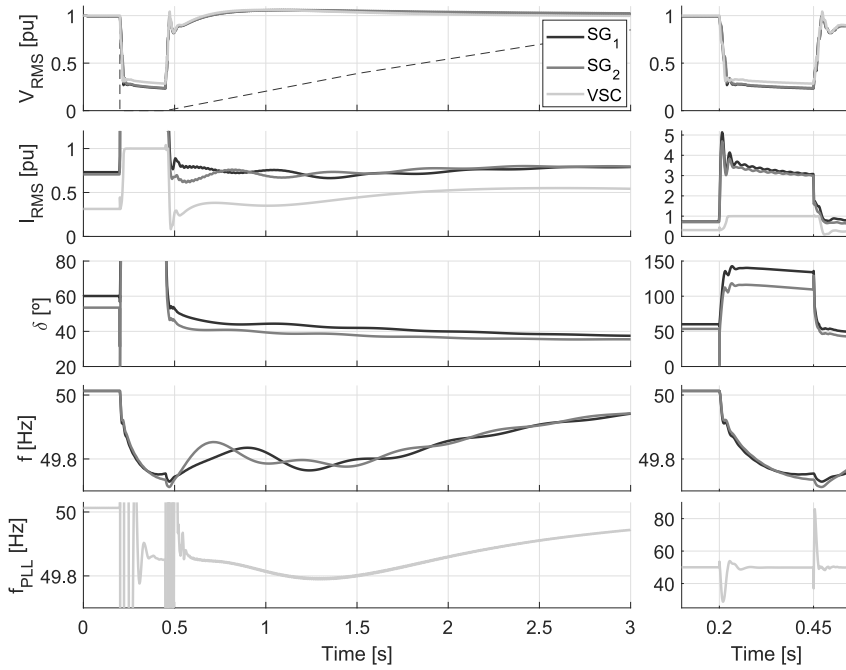
Fig. 7. Results of Case 1 after a fault in bus 6.
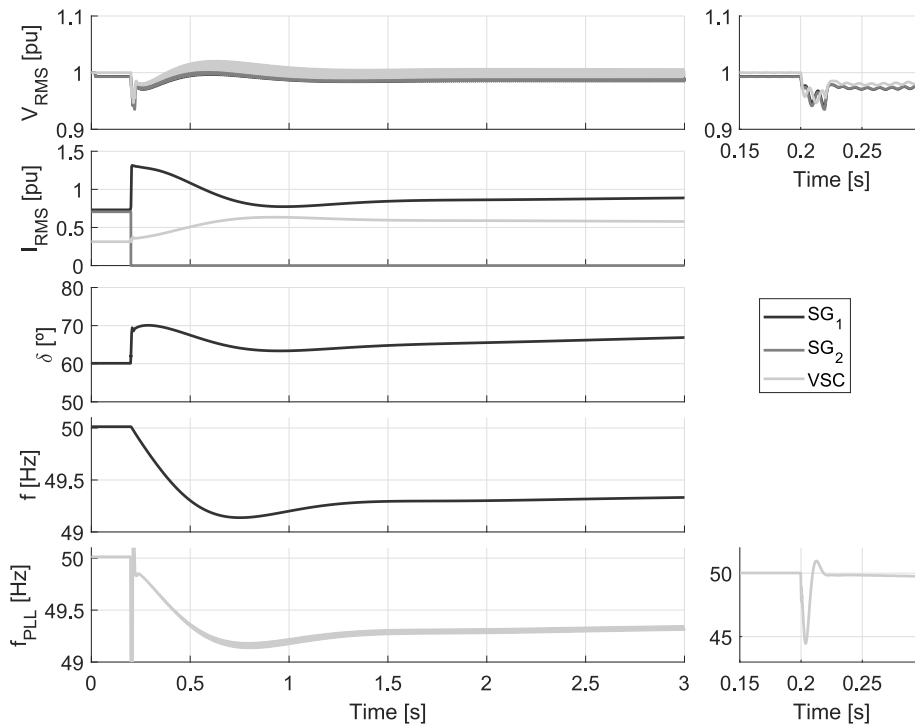
Fig. 8. Results of Case 1 after the disconnection of SG2.

saturates current at 1 pu, while the SGs provide the fault current, injecting around 5 pu, as shown in Fig. 7. This is directly indicated by the current indices in Fig. 9, DCI$_{VSC}$ and DCI$_{SG}$. Due to the high SG current injection during the fault, the ROCOF reaches a maximum value around 0.6 Hz/s. As the fault is a short-time event, the maximum frequency deviation is not very remarkable, being less than 0.3 Hz. Both frequency-related values are within the accepted ranges defined in Section 2, which is also observed from the FDI and MFDI in Fig. 9 with values around 0.3. Although the rotor angles reach high values during the fault, the SGs keep synchronism after the fault clearance, leading to

a DGAI around 0.6. The PLL also keeps the VSC synchronised with the system despite of the sharp voltage variations during the fault, which is reflected in the PLLI with a value equal to 0.2. Finally, the overvoltage after the fault clearance is up to 1.05 pu, *i.e.* the voltage is kept within the limits and results in a DVI equal to 0.5. Therefore, even though the current-related indices show a high increase of SG current, the rest of the indices are under the defined limits, which is translated in a stable transient operation.

The disconnection of the SG2 implies a reduction of the system inertia to half of the initial value, as well as a 35% loss of the
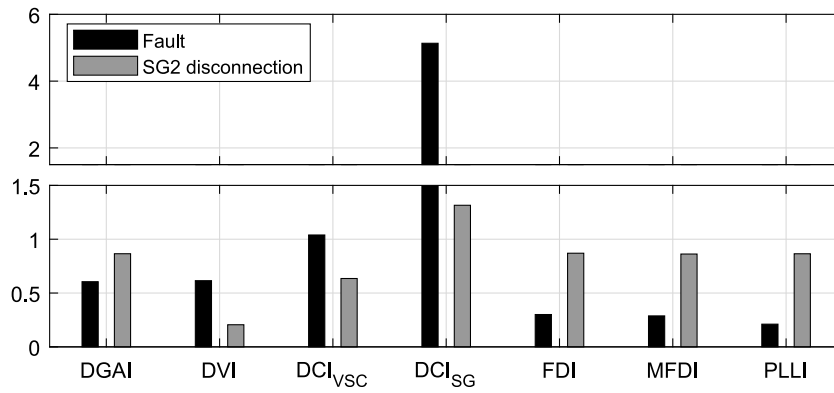
Fig. 9. Transient indices obtained for Case 1.
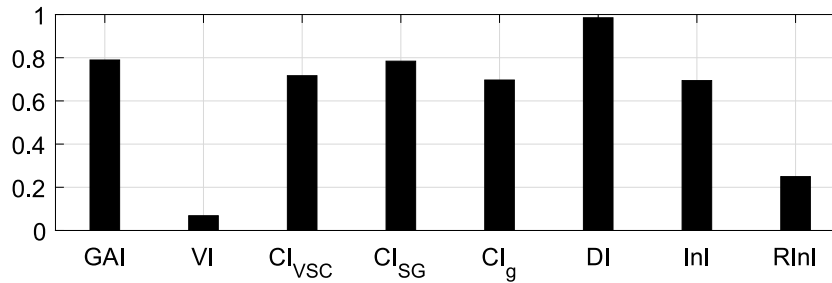
(a) Steady-state and small-signal indices
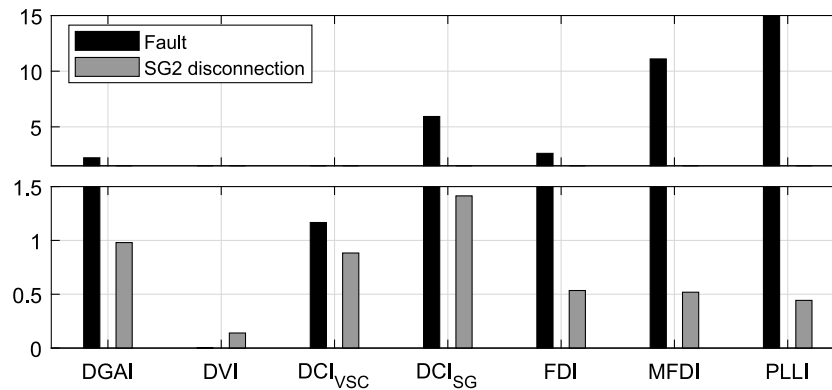
(b) Transient indices

Fig. 10. Indices from Case 2.

total active power generation, leading to higher values for frequency-related indices. The FDI is close to 1, almost exceeding the maximum admissible ROCOF of 2 H/s, while the MFDI is equal to 0.85, which indicates that frequency nadir is also lower than in the fault case, reaching around 49.15 Hz. The rest of the transient indices do not show abnormal operation, which confirm a stable operation.

3.2. Case 2: reduction of synchronous generation

In this case, the rated power of each SG is reduced to 100 MVA, as shown in Table 1. Then, the SGs provide 140 MW (28%) of the total demand, while the VSC supplies the remaining 360 MW (72%).

Steady-state and small-signal indices, shown in Fig. 10(a), reveal an adequate operation of the system. In this case, the CI_{VSC} is much higher, increasing from 0.31 in Case 1 to 0.72 in Case 2, as the VSC compensates the SG generation reduction increasing its active power injection. The maximum RInI is 0.25, which is also higher than in Case 1, denoting the presence of interactions with higher risk of

instability. However, this RInI is still low enough to ensure stability. The remaining indices are similar to Case 1.

Regarding the transient operation, the system is not stable due to the fault at bus 6. The VSC does not keep synchronism, since the PLL frequency rapidly drops from 50 Hz, as shown in Fig. 11. This is observed in the PLLI, which is widely exceeding the admissible limits as seen in Fig. 10(b). The indices related to the SG frequency, *i.e.* FDI and MFDI, are also greater than 1, but lower than the PLLI, indicating that the VSC is the element that causes the system instability. Otherwise, the PLLI would be equal to the FDI, showing that the VSC is synchronised even after a large deviation of the frequency, as in Case 1. Additionally, as the voltage does not recover after the fault, the DVI is equal to 0.

When the SG2 disconnection is produced, only the 14% of the active power is lost from the system. This active power unbalance is lower than in Case 1, when the active power loss was 35%. Then, even though the system has lower inertia than in Case 1, the VSC can compensate this active power loss with less frequency deviation. This can be observed in Fig. 10(b), which shows the FDI and MFDI for this
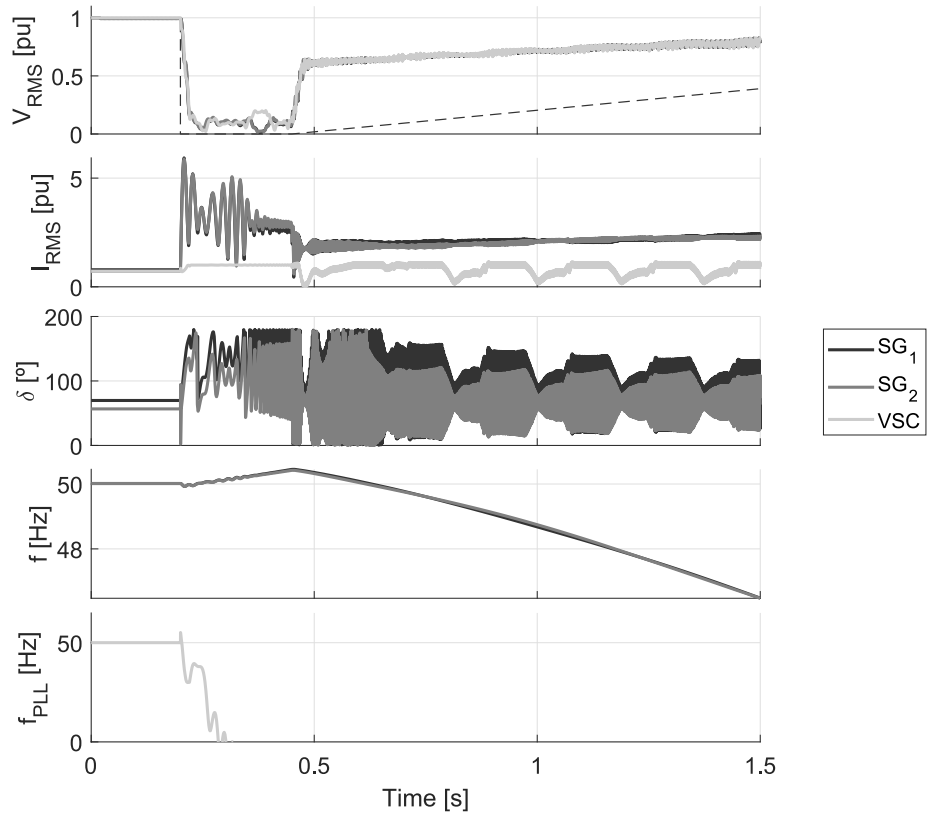
Fig. 11. Results of Case 2 after a fault in bus 6.

(a) Steady state indices. Colour code: ● No LF solution has been found; ● Steady-state limit violation (index>1)

(b) Small-signal indices. Colour code: ● Steady-state unfeasible operation point
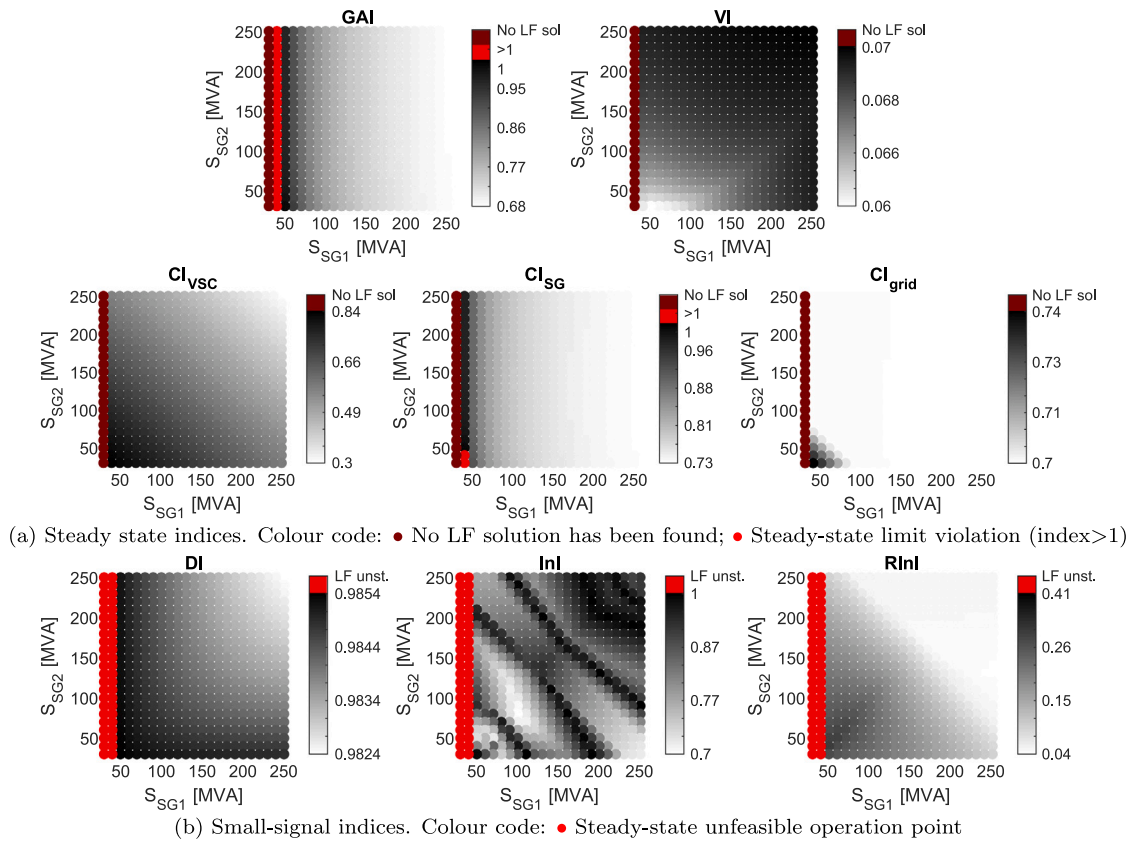
Fig. 12. Steady state and small-signal indices when the SG presence is reduced in the system.

(a) Fault in bus 6

(b) SG2 disconnection

(c) SG1 disconnection
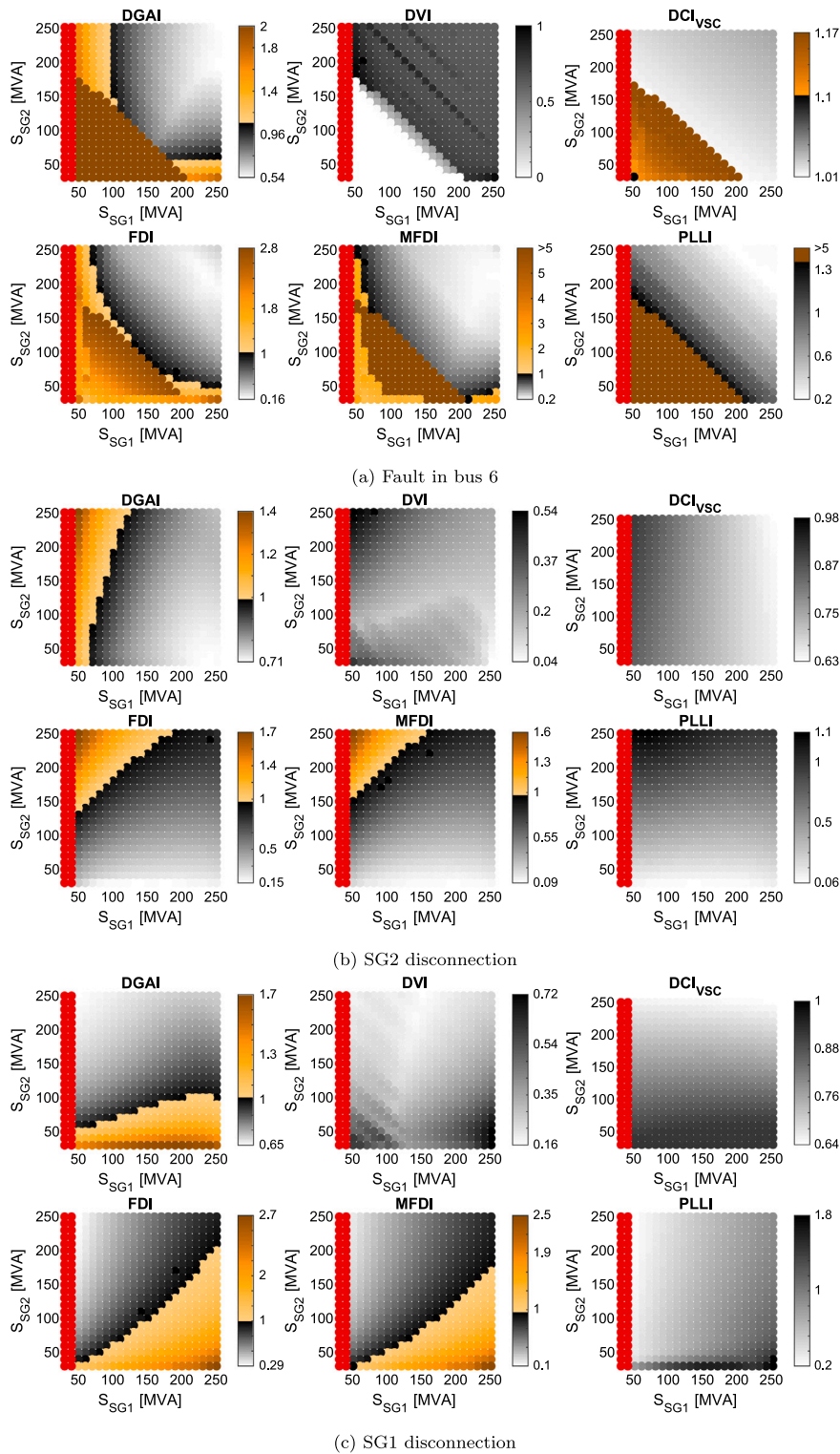
Fig. 13. Transient indices when the SG presence is reduced in the system. Colour code: • Steady-state unfeasible operation point.

Case 2, which are around 0.5, while these indices were above 0.8 for Case 1.

4. Stability and operation limits when the SG presence is reduced

In this section, the system stability and operation limits have been studied when the synchronous generation is progressively reduced in the 9-bus power system presented in Fig. 3(a). In particular, the rated power of both SG1 and SG2 is reduced from 250 MVA to 30 MVA in intervals of 10 MVA, resulting in 529 cases. As in Section 3, the SG power references are set to 70% of their rated power, while the VSC provides the rest of the demand.

Figs. 12 and 13 show the performance indices obtained for all the combinations. The indices are represented with a colour code, where those depicted in a greyscale correspond to stable cases, *i.e.* indices

lower than 1, while those represented in different tones of red or orange correspond to a limit violation or instability, *i.e.* indices higher than 1.

The indices from the steady-state analysis show several cases where the Load Flow (LF) algorithm cannot find a solution, which are represented with dark red bullets (•) in Fig. 12(a). In addition, several unstable cases are also found, which correspond to some limit violation. These instabilities are related to the generator angle (GAI) and are depicted in red (•) in Fig. 12(a). As shown in Table 2, the SG1 reactive power absorption is higher compared to SG2. When the SG1 rated power is reduced, the maximum generator angle increases due to the high reactive power exchange of SG1, resulting in a steady-state rotor angle instability. This is observed in the GAI, which changes from white (minimum value, GAI=0.68) to black (GAI=1) and finally red (GAI>1) at the left side (lowest SG1 power). The load flow has been run considering a terminal voltage for the SGs and the VSC equal to 1 pu. Adapting these voltage references could also lead to different results, reducing the reactive power needed from SG1. Regarding the VSC, the CI_{VSC} index reveals that the VSC compensates the demand when the SGs are reduced. The voltage deviation is very reduced, since the VI is between 0.06 and 0.07.

The indices derived from the small-signal analysis are depicted in Fig. 12(b), which include the non-feasible steady-state operation points (depicted with red bullets •). The small-signal analysis does not reveal any additional unstable case, *i.e.* DI is lower than 1 for all cases. The InI exposes a high variability in the maximum interaction between the SGs and the VSC when the SG power is reduced. This might be caused due to different interaction mechanisms, *e.g.* interactions related to currents, voltage or PLL, whose dominance changes throughout the SG power variation. The RInI reveals a clear tendency, as the interactions have higher risk of instability when the SG size is reduced. However, RInI does not show which specific interaction is causing problems. This has to be confirmed by analysing the poles and PF matrix of the specific cases.

Regarding the transient analysis, the events considered in Section 3 were a fault at bus 6 and the SG2 disconnection to study two particular cases, Case 1 and Case 2. In this Section 4, these two events are also considered, but also adding the SG1 disconnection. The fault indices in Fig. 13(a) show a large amount of unstable cases, represented in dark orange (•), which correspond to a VSC loss of synchronism, as the PLL does not follow the actual frequency due to the large deviation of the voltage. This can be observed in the PLLI, whose unstable cases are represented in dark orange (•) with values higher than 5. These instabilities are mapped in all the indices, as all the magnitudes of the system are affected by the VSC instability. For example, the voltage does not recover after the fault, so this area in the DVI is depicted as white (DVI=0). A number of stable cases show a high ROCOF, which is observed in the FDI, where many cases are represented in an orange gradient, corresponding to a violation of the 2 Hz/s limit.

The SG2 disconnection indices in Fig. 13(b) does not reveal any unstable case, but many frequency protection violations. This frequency limits violation are observed in FDI and MFDI, which show many cases with values above 1. Similar results are obtained for the SG1 disconnection. The indices in Fig. 13(c) are roughly symmetrical respect to the SG2 disconnection in Fig. 13(b).

Combining all the results, a global system stability map is depicted in Fig. 14, where each area corresponds to different instabilities or limit violations. The stable area is depicted in green, which fulfils all the transient requirements. Many cases are defined as quasi-stable in Fig. 14, which means they are stable, but exceed frequency protection limits. A distinction is considered for cases where only the FDI is exceeded (depicted in clear green) or both FDI and MFDI are violated (in clear orange). Note that modifying the frequency protection criteria could extend the stable area. The orange area refers to unstable cases after a transient event, which correspond to a VSC loss of synchronism after the fault. This transient instability area could be modified by changing the PLL implementation or design, *e.g.* including PLL blocking during the fault. The steady-state and small-signal analysis have been carried out for specific power flow conditions. This unstable area might also differ if the operation points of the VSC and SGs are modified.
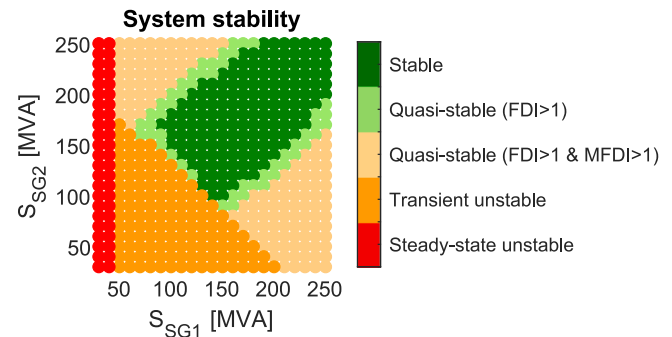
Fig. 14. System stability when the SG presence is reduced.

5. Conclusions

In this paper, the stability and operation limits have been analysed in power systems with high VSC penetration and reduced synchronous generation. In particular, the minimum synchronous generation that ensures a proper operation has been evaluated in a system with a VSC-HVDC link considering steady-state, small-signal and transient analysis. This study finally provides a stable operation area for the power system, identifying also different areas according to the steady-state, small-signal and transient stability and operation limits. The transient stability was found to be the most restrictive aspect. Specifically, the frequency protections limits are exceeded when a fault or a SG disconnection is produced in cases with low SG presence. In case of fault, the VSC losses synchronism when the rated power of the SG is reduced, providing less short-circuit power and resulting in deeper faults. Despite the minimum SG presence required for stability may depend on the particular system, with a specific grid topology or converter control algorithms, the results obtained indicate a clear trend about potential issues when the SG is reduced.

This analysis has been carried out using performance indices, which evaluate many magnitudes of the system, such the bus voltages, generator frequencies, currents in every element or the minimum damping of the linearised model. The use of these indices provides a complete overview of the power system operation, leading to save analysis time of power system engineers, as the combination of indices allows identifying critical cases that can be eventually studied in detail. In addition, the performance indices can be applied to any power system, considering different control approaches and protection algorithms. Other elements, such as Line-Commutated Converters, could be also included in the study, which may introduce new indices to consider their performance. For large systems with multiple generators and converters, these indices can be used to obtain a multidimensional map, where steady-state, small-signal and transient unstable operation regions can be identified.

CRediT authorship contribution statement

Carlos Collados-Rodriguez: Conceptualisation, Methodology, Software, Writing – original draft, Writing – review & editing. **Marc Cheah-Mane:** Conceptualisation, Supervision, Writing – original draft, Writing – review & editing. **Eduardo Prieto-Araujo:** Conceptualisation, Supervision. **Oriol Gomis-Bellmunt:** Conceptualisation, Supervision, Writing – review & editing.

Declaration of competing interest

The authors declare that they have no known competing financial interests or personal relationships that could have appeared to influence the work reported in this paper.

Acknowledgments

References

[1] Wang L, Xie X, Jiang Q, Liu H, Li Y, et al. Investigation of SSR in practical DFIG-based wind farms connected to a series-compensated power system. IEEE Trans Power Syst 2015;30(5):2772–9. http://dx.doi.org/10.1109/TPWRS.2014.2365197.

[2] Liu H, Xie X, Gao X, Liu H, Li Y. Stability analysis of SSR in multiple wind farms connected to series-compensated systems using impedance network model. IEEE Trans Power Syst 2018;33(3):3118–28. http://dx.doi.org/10.1109/TPWRS.2017.2764159.

[3] Sun J, Li M, Zhang Z, Xu T, He J, et al. Renewable energy transmission by HVDC across the continent: system challenges and opportunities. CSEE J Power Energy Syst 2017;3(4):353–64. http://dx.doi.org/10.17775/cseejpes.2017.01200.

[4] Buchhagen C, Rauscher C, Menze A, Jung J. BorWin1 - first experiences with harmonic interactions in converter dominated grids. In: International ETG congress 2015. (Bonn, Germany), 2015.

[5] AEMO. Black system South Australia 28 September 2016. Tech. rep, 2017, March.

[6] AEMO. Final report – Queensland and South Australia system separation on 25 August 2018. Tech. rep, 2019, January.

[7] National Grid ESO. Technical report on the events of 9 August 2019. Tech. rep, 2019, September.

[8] EirGrid and SONI. All island TSO facilitation of renewables studies. Tech. rep, 2010.

[9] Vittal E, O'Malley M, Keane A. A steady-state voltage stability analysis of power systems with high penetrations of wind. IEEE Trans Power Syst 2010;25(1):433–42. http://dx.doi.org/10.1109/TPWRS.2009.2031491.

[10] O'Sullivan J, Rogers A, Flynn D, Smith P, Mullane A, et al. Studying the maximum instantaneous non-synchronous generation in an island system - Frequency stability challenges in Ireland. IEEE Trans Power Syst 2014;29(6):2943–51. http://dx.doi.org/10.1109/TPWRS.2014.2316974.

[11] Alsokhiry F, Adam GP, Al-Turki Y. Limitations of voltage source converter in weak ac networks from voltage stability point of view. Int J Electr Power Energy Syst 2020;119(July 2020):105899. http://dx.doi.org/10.1016/j.ijepes.2020.105899.

[12] Delille G, François B, Malarange G. Dynamic frequency control support by energy storage to reduce the impact of wind and solar generation on isolated power system's inertia. IEEE Trans Sustain Energy 2012;3(4):931–9. http://dx.doi.org/10.1109/TSTE.2012.2205025.

[13] Gautam D, Vittal V, Harbour T. Impact of increased penetration of DFIG-based wind turbine generators on transient and small signal stability of power systems. IEEE Trans Power Syst 2009;24(3):1426–34. http://dx.doi.org/10.1109/TPWRS.2009.2021234.

[14] Eftekharnejad S, Vittal V, Heydt GT, Keel B, Loehr J. Small signal stability assessment of power systems with increased penetration of photovoltaic generation: A case study. IEEE Trans Sustain Energy 2013;4(4):960–7. http://dx.doi.org/10.1109/TSTE.2013.2259602.

[15] Edrah M, Zhao X, Hung W, Qi P, Marshall B, et al. Electromechanical interactions of full scale converter wind turbine with power oscillation damping and inertia control. Int J Electr Power Energy Syst 2022;135(February 2022):107522. http://dx.doi.org/10.1016/j.ijepes.2021.107522.

[16] Collados-Rodriguez C, Cheah-Mane M, Prieto-Araujo E, Gomis-Bellmunt O. Stability analysis of systems with high VSC penetration: where is the limit? IEEE Trans Power Deliv 2020;35(4):2021–31. http://dx.doi.org/10.1109/TPWRD.2019.2959541.

[17] IEEE Power and Energy Society. IEEE recommended practice for excitation system models for power system stability studies. Tech. rep, 2016.

[18] Henninger S, Jaeger J. Advanced classification of converter control concepts for integration in electrical power systems. Int J Electr Power Energy Syst 2020;123(December 2020):106210. http://dx.doi.org/10.1016/j.ijepes.2020.106210.

[19] Morren J, de Haan SW, Kling WL, Ferreira JA. Wind turbines emulating inertia and supporting primary frequency control. IEEE Trans Power Syst 2006;21(1):433–4. http://dx.doi.org/10.1109/TPWRS.2005.861956.

[20] Kundur P. Power system stability and control. McGraw-Hill; 1994.

[21] Gimenez Alvarez JM, Mercado PE. Online inference of the dynamic security level of power systems using fuzzy techniques. IEEE Trans Power Syst 2007;22(2):717–26. http://dx.doi.org/10.1109/TPWRS.2007.895161.

[22] EirGrid. EirGrid grid code. Tech. rep, 2019, June.

[23] National Grid. The grid code. Tech. rep, 2020, November.

[24] ENTSO-E. Frequency stability evaluation criteria for the synchronous zone of continental europe. Tech. rep, 2016, March.

[25] DNV KEMA, EirGrid. RoCoF: An independent analysis on the ability of generators to ride through rate of change of frequency values up to 2 Hz/s.. Tech. rep, 2013, February.

[26] Wang X, Taul MG, Wu H, Liao Y, Blaabjerg F, et al. Grid-synchronization stability of converter-based resources—An overview. IEEE Open J Ind Appl 2020;1:115–34. http://dx.doi.org/10.1109/ojia.2020.3020392.

[27] Taul MG, Wang X, Davari P, Blaabjerg F. An overview of assessment methods for synchronization stability of grid-connected converters under severe symmetrical grid faults. IEEE Trans Power Electron 2019;34(10):9655–70. http://dx.doi.org/10.1109/TPEL.2019.2892142.